[AMERICAN JOURNAL OF SCIENCE, VOL. 277, APRIL, 1977, P. 353-383]

American Journal of Science

APRIL 1977

MINERAL EQUILIBRIA IN THE MgO–SiO_2–H_2O SYSTEM: II TALC–ANTIGORITE–FORSTERITE–ANTHOPHYLLITE–ENSTATITE STABILITY RELATIONS AND SOME GEOLOGIC IMPLICATIONS IN THE SYSTEM

J. J. HEMLEY*, J. W. MONTOYA**,
D. R. SHAW*, and R. W. LUCE*

ABSTRACT. Mineral equilibria in the MgO–SiO_2–H_2O system were investigated, with emphasis on the stability relations of talc, antigorite, forsterite, anthophyllite, and enstatite. Thermal dehydration temperatures at 1 kb H_2O are at 514° ± 12°C (Ta–Antig–Fo), 627° ± 7°C (Ta–Fo–Anth), 670° ± 7°C (Anth–Fo–En), 675° ± 7°C (Ta–Anth–Q), 643° ± 8°C (Ta–Fo–En), 690° ± 8°C (Ta–En–Q), 729° ± 8°C (Anth–En–Q). Derived $G°_f$ values in kcal/gf are −928.756 ± 1.1 (Antig, based on $Mg_{2.825}Si_2O_5(OH)_{3.65}$), −2711.320 ± 1.7 (Anth) and −348.955 ± 0.6 (En). Anthophyllite has a relatively narrow temperature stability range at 1 kb, but it increases as P_{H_2O} increases.

The Ta–Fo–En and Ta–En–Q reactions are low-pressure changes, metastable at 1 kb. The (Q) and (Fo) invariant points are at approximately 603°C, 500 bars, and 601°C, 175 bars, P_{H_2O}, respectively. Higher P_{total} raises and spreads the P_{H_2O} values of the invariant points.

The log $SiO_{2\,aq}$ versus 1/T diagrams utilized in this study are applied to metasomatic and isochemical processes involving this system. Aspects of contact metamorphism and metasomatism, the process of serpentinization, and compositional controls and relative stabilities of the serpentine phases are discussed. Isochemical cooling in the subsolidus at finite, though not necessarily constant, P_{H_2O} results in a mineral reaction series analogous to that of the classical reaction series of silicate melts, with significant implications to deuteric alteration and retrograde metamorphism.

The chemical constraints revealed in the various equilibria studied, focusing on nonisochemical reactions and considering the effects of changing pressure, help to clarify and more rigorously to define the isochemical PT relationships of the system. The geological application of activity-activity or chemical potential diagrams is also discussed, and the necessity of considering reactions that correspond to or approximate the true process involved is illustrated.

INTRODUCTION

The basic purposes, experimental procedures, and low-temperature stability relations involved in this study have been presented in the preceding paper (Hemley and others, 1977). In this paper, additional equilibria and various geological implications are discussed. Phase relations for minerals of major interest in the MgO–SiO_2–H_2O system are given in figure 1.

UNITS, ABBREVIATIONS, AND MINERAL FORMULAE

$G°_f$, $H°_f$, $S°_f$ Standard (298 K, 1 bar) gram-formula Gibbs free energy, enthalpy, and entropy of formation of a phase from the elements.

* U.S. Geological Survey, 959 National Center, Reston, Virginia 22092.
** 1524 South Aida Avenue, Tucson, Arizona 85710

cal, kcal	Unit of energy, 1 cal = 4.184 joules.
Cp	Heat capacity of a substance, cal/deg.
gf	Unit gram formula weight of a substance.
cal/bar	Unit of volume, 1 cal/bar = 41.842 cc.
S°	Standard (298 K, 1 bar) ("Third Law") entropy of a phase.
T, t	Temperature in kelvins (K) or degrees celsius (°C), as specified.
P	Pressure in bars or kilobars (kb), as specified.
$\Delta S^\circ_{f,s}$	Difference in entropy of formation of product and reactant solids for a given reaction.
ΔV_s	Difference in volume of product and reactant solids.
m	Molality of a component.
[ ]	Activity of a component.
f	Fugacity of a component.
μ	Chemical potential of a component. $\mu = \mu_o + RT \ln a = \mu_o + RT \ln \frac{f}{f_o}$, where the subscript o refers to the standard state.

$G^*_{H_2O}(T_e,P_e) = G^\circ_f(H_2O)(T_e,1\text{ bar}) + G(H_2O)(T_e,P_e) - G(H_2O)(T_e,1\text{ bar})$ (Fisher and Zen, 1971).

Talc	$Mg_3Si_4O_{10}(OH)_2$
Sepiolite	$Mg_2Si_3O_{7.5}(OH) \cdot 3H_2O$
Chrysotile	$Mg_3Si_2O_5(OH)_4$
Antigorite	$Mg_3Si_2O_5(OH)_4$ (approx)
Forsterite	Mg_2SiO_4
Anthophyllite	$Mg_7Si_8O_{22}(OH)_2$
Enstatite	$MgSiO_3$

STABILITY OF ANTIGORITE AND SEPIOLITE

Compositions and X-ray character of the phases used in the investigation of antigorite are given in table 1. The equilibrium results are given in table 2 and plotted in figure 1. The antigorite–talc pairs show higher aqueous silica values than the corresponding chrysotile–talc equilibrium. The result is a higher temperature intercept with the talc–forsterite boundary. This higher decomposition temperature for antigorite relative to chrysotile is in better accord with metamorphic field relations and has been tacitly assumed as true by field geologists for many years. The value indicated in figure 1, 514° ± 12°C, is in good agreement with the extrapolation of the curve of Johannes (1975) based on higher pressure determinations, although reversals are difficult to demonstrate for talc–antigorite, and more data points at long run times would be desirable.

The relationship of antigorite to chrysotile has been the subject of considerable mineralogical discussion. As suggested by Page (1968), the minerals probably should not be considered polymorphs. Antigorite, with rare exceptions, has a relatively high iron and/or aluminum content, whereas chrysotile characteristically has distinctly lower values. Probably

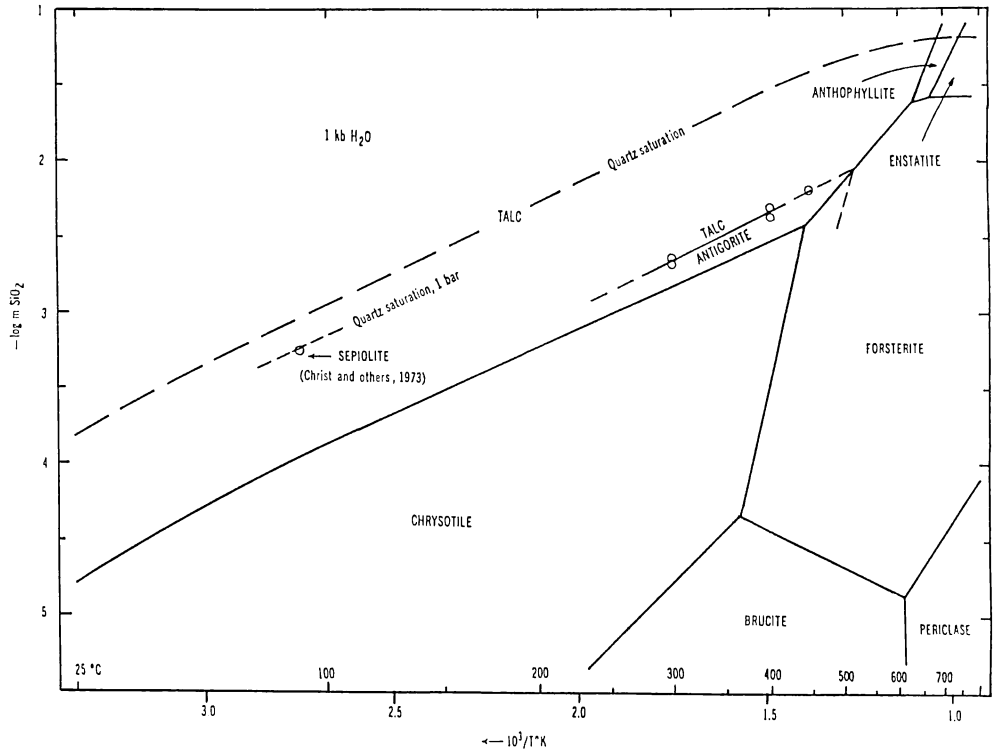

Fig. 1 Mineral stability relations in the system MgO–SiO_2–H_2O as a function of log $mSiO_2$ versus 1/T, at 1 kb H_2O. Relationships among talc, chrysotile, forsterite, brucite, and periclase are from Hemley and others, 1977.

more important, antigorites show slightly higher SiO_2 and lower H_2O content (Faust and Fahey, 1962; Whittaker and Wicks, 1970), indicative of a modified bonding relationship in the structure (Kunze, 1961, 1958). These differences, one may argue, result in distinct phases with appreciably different thermal stabilities. Occasional overlap in composition would not necessarily invalidate such an interpretation in view of the fairly common occurrence of metastability in lower grade metamorphic and alteration assemblages. This applies even more strongly to mineral synthesis. Whether or not antigorite is to be regarded as a polymorph of chrysotile, it is, apparently, the more stable phase over much or most of the temperature range in figure 1. Antigorite–chrysotile relationships are discussed further in a later section.

The Gibbs free energy of formation of antigorite was calculated from the talc–antigorite–forsterite intercept in figure 1. Assigning the composition of ideal chrysotile to antigorite, the reaction is

$$5 \text{ antigorite} = \text{talc} + 6 \text{ forsterite} + 9\ H_2O. \qquad (1)$$

TABLE 1

Chemical analyses and X-ray data

Oxide* (wt %)	Talc natural (1)	Antigorite natural (2)	Enstatite natural (3)	Anthophyllite natural (4)	Talc natural (1) dA°	I/II	hkl	Talc synthetic (5) dA°	I/II	hkl	Forsterite synthetic (6) dA°	I/II	hkl
SiO_2	62.5	43.1	58.7	61.0	9.35	100	002	9.35	100	002	5.09	50	020
MgO	30.9	39.8	38.8	29.2	4.67	8	004	4.67	8	004	3.87	70	021
FeO**	1.13	3.7	2.6 (1.0)***	5.9 (2.9)	4.59	45	020	4.59	45	020	3.47	20	120
Al_2O_3	0.33	1.3	0.11	0.33	4.56	25	$11\bar{1}$	4.56	25	$11\bar{1}$	2.76	60	130
CaO	0.11	0.02	0.0	0.58 (.42)	4.53	12	110	4.53	12	110	2.50	70	131
Na_2O	0.45	—	0.0	0.0	3.12	40	$11\bar{5}$	3.12	40	$11\bar{5}$	2.457	100	112
K_2O	0.09	—	0.0	0.0	2.338	2	008	2.589	14	131	2.34	20	041
MnO	0.0	0.03	0.0	0.16	1.869	4	$20\bar{8}$	2.479	30	$13\bar{2}$	2.26	40	122
Cr_2O_3	—	0.06	—	—	1.558	2	$31\bar{7}$	1.876	4	$20\bar{8}$	2.245	30	140
NiO	—	0.11	—	—	1.529	55	060	1.529	55	060	1.749	40	222
H_2O^+	4.2	11.9	—	2.50	a = 5.29, b = 9.18,			a = 5.29, b = 9.17,			1.495	20	004
H_2O^-	0.15	0.07	—	—	c = 18.98, β = 100°10′			c = 18.96, β = 100°5′			1.478	20	062
											a = 4.75, b = 10.18, c = 5.976		

Antigorite natural (2)			Enstatite natural (3)			Enstatite synthetic (7)			Anthophyllite natural (4)		
dA°	I/II	hkl	dA°	I/II	hkl	dA°	I/II	hkl	dA°	I/II	hkl
7.37		001	3.16	75	420	4.39 (4.38)	20	020	9.30	25	200
4.61		020	3.14	50	221	3.165 (3.16)	75	420	8.93 (8.90)	30	020
3.66		002	2.930	14	321	3.145 (3.14)	50	221	8.19 (8.26)	55	210
2.669		200	2.86	100	610	2.868 (2.86)	100	610	5.01 (5.03)	14	101, 011
2.504		131	2.70	10	421	2.698 (2.69)	8	421	4.61 (4.62)	14	400, 201
2.455		003	2.528	18	131	2.528 (2.528)	18	131	4.48 (4.49)	25	400, 201
2.095		204	2.488	8	202	2.488 (2.488)	8	202	4.10 (4.10)	20	420
1.539		060	2.464	10	521	2.461 (2.461)	10	521	3.61 (3.64)	35	321, 231, 430
1.505		061	2.08	12	531	2.108 (2.108)	8	630	3.338 (3.33)	30	141, 250, 411
1.459		005	1.952	10	631	1.977 (1.977)	4	241	3.21 (3.22)	60	421, 440
1.417		062	1.518	14	12.00	1.956 (1.952)	10	631	3.03 (3.04)	100	610, 501
1.279		170	1.484	20	10.31	1.481 (1.483)	20	10.31	2.866 (2.865)	20	521
a = 43.53, b = 9.259,			1.469	15	060	1.469	25	060	2.822 (2.830)	40	450, 260
c = 7.263, β = 98°8.4′			a = 18.20, b = 8.80,			a = 18.20, b = 8.80, c = 5.167			2.738 (2.739)	20	411, 630
			c = 5.163						2.674 (2.676)	30	531, 351
									2.574 (2.570)	30	102, 161, 112
									2.528 (2.528)	40	621, 640
									a = 18.49, b = 17.81, c = 5.26		

Sources: (1) New South Wales, Australia; (2) New Zealand (Page and Coleman, 1967); (3) Bamle, Norway; (4) Minneapolis, N.C.; (5) 500°C, 1 kb, 14 days; (6) 650°C, 0.5 kb, 5 days; (7) 780°C, 0.5 kb, 5 days.

* S. D. Botts and Leonard Shapiro, analysts.

** Total Fe as FeO.

*** Parentheses for material exchanged in 1 m $MgCl_2$, 720°C, 2 kb, 5 days.

TABLE 2
Equilibrium concentration data, 1 kb

Temp. (°C)	Initial charge: Solids	Initial charge: $-\log mSiO_2$	Equilibrium $SiO_{2\,aq}$ $-\log mSiO_2$	Time (days)
300	Talc–Antigorite	H_2O	2.60	60
300	Talc–Antigorite	2.60	2.64	60
400	Talc–Antigorite	H_2O	2.30	30
400	Talc–Antigorite	2.30	2.36	30
450	Talc–Antigorite	H_2O	2.20	30
550	Talc–Forsterite	H_2O	1.87	10
600	Talc–Forsterite	1.77	1.72	5
600	Talc–Forsterite	H_2O	1.73	5
640	Talc–Forsterite	2.30	1.62	9
640	Talc–Forsterite	1.33	1.63	3
640	Talc–Anthophyllite	H_2O	1.59	3
650	Talc–Anthophyllite	1.33	1.50	9
660	Talc–Anthophyllite	H_2O	1.40	4
660	Talc–Anthophyllite	1.80	1.40	5
670	Talc–Anthophyllite	1.50	1.27	4
670	Talc–Anthophyllite	1.33	1.31	4
670	Talc–Anthophyllite	1.38	1.30	3
649	Talc–Enstatite	1.33	1.58	7
650	Talc–Enstatite	1.33	1.55	7
662	Talc–Enstatite	H_2O	1.48	4
659	Talc–Enstatite	H_2O	1.43	4
670	Talc–Enstatite	1.52	1.39	4
670	Talc–Enstatite	1.38	1.40	5
685	Talc–Enstatite	1.78	1.33	5
690	Talc–Enstatite	1.33	1.20	5
650	Anthophyllite–Forsterite	1.33	1.61	5
670	Anthophyllite–Forsterite	1.68	1.53	4
670	Anthophyllite–Forsterite	1.33	1.57	4
670	Anthophyllite–Forsterite	1.68	1.57	5
660	Anthophyllite–Enstatite	1.78	1.60	5
670	Anthophyllite–Enstatite	1.33	1.54	4
670	Anthophyllite–Enstatite	1.68	1.55	3
670	Anthophyllite–Enstatite	1.63	1.58	5
680	Anthophyllite–Enstatite	1.68	1.51	1
680	Anthophyllite–Enstatite	1.33	1.53	4
690	Anthophyllite–Enstatite	1.68	1.46	4
690	Anthophyllite–Enstatite	1.68	1.51	4
700	Anthophyllite–Enstatite	1.60	1.44	6
700	Anthophyllite–Enstatite	1.60	1.60	6
700	Anthophyllite–Enstatite	1.38	1.39	7
715	Anthophyllite–Enstatite	1.38	1.42	1
715	Anthophyllite–Enstatite	1.50	1.48	5
715	Anthophyllite–Enstatite	1.50	1.38	5
680	Enstatite–Forsterite	H_2O	1.53	1
680	Enstatite–Forsterite	1.69	1.56	4
685	Enstatite–Forsterite	1.77	1.57	5
690	Enstatite–Forsterite	1.69	1.53	4
700	Enstatite–Forsterite	1.33	1.57	7
720	Enstatite–Forsterite	1.65	1.55	5
720	Enstatite–Forsterite	1.33	1.58	5

The calculation proceeds as follows:

$$\Delta Gr(T_e,1000) = 0 = G°_f(298,1)_{Ta} + 6G°_f(298,1)_{Fo} - 5G°_f(298,1)_{Antig} + 9G^*_f(T_e,1000)_{H_2O} + 999\Delta V_s - \Delta S°(298)_{f,s}\Delta T + \int_{298}^{T_e} \Delta Cp_{f,s}dT - T_e \int_{298}^{T_e} \Delta Cp_{f,s}d\ln T. \quad (2)$$

The quantity $-\Delta S°(298)_{f,s}\Delta T + \int\Delta Cp_{f,s}dT - T_e\int\Delta Cp_{f,s}d\ln T$ constitutes the temperature correction on the free energy of formation of the solids at higher temperature and 1 bar. Eq 2 is used in all subsequent calculations of Gibbs free energy of formation in the present paper. The two integrated terms in eq (2) are, respectively,

$$a\Delta T + \frac{b}{2}(T_e^2 - 298.15^2)\,10^{-3} - c\left(\frac{1}{T_e} - \frac{1}{298.15}\right)10^5$$

and

$$-T_e\left[a\ln\frac{T_e}{298.15} + b\Delta T\,10^{-3} - \frac{c}{2}\left(\frac{1}{T_e^2} - \frac{1}{298.15^2}\right)10^5\right],$$

where a, b, and c are the sum of the heat capacity constants for the reaction, as given in table 3. For eq (1), the value of $\Delta Cp_{f,s}$ is given by $Cp_{Ta} + 6Cp_{Fo} - 5Cp_{Antig} + 9CpH_2 + 9/2\ CpO_2$. Values of $G^*_{H_2O}$ are from Fisher and Zen (1971). The calculated free energy value is -966.728 ± 1.1 kcal/gf.

A preferable free energy value is obtained using a more appropriate composition for antigorite, such as the idealized structural composition $Mg_{2.825}Si_2O_5(OH)_{3.65}$, simplified from Kunze (1956). The reaction is then

$$5 \text{ antigorite} = 1.175 \text{ talc} + 5.3 \text{ forsterite} + 7.95\ H_2O. \quad (1A)$$

Using the data in table 3, the calculated free energy is -928.756 ± 1.1 kcal/gf. No adjustments were made in the molar entropy and volume for the small change in gram formula weight of the antigorite, and no estimate was made for the free energy difference between the natural material used and the ideal pure-Mg end-member. These adjustments tend to cancel and do not appear justified in view of the considerable uncertainty already present in the experimental and thermodynamic data. The free energy contribution of the variable, but appreciable, Fe and Al content of antigorite is yet to be established, and calorimetric evaluations are very much in order. The natural material probably should not be used as a basis for the above equation, (1A), without further analytical corroboration of its composition. Its formula corresponds approximately to $Mg_{2.89}Si_{1.93}O_5(OH)_{3.56}$. The formula may be recast to approximate better the idealized composition give above by assigning a large portion

TABLE 3

	G°_f (kcal/gf)	S° (cal/deg gf)	S°_f (cal/deg gf)
Forsterite	−491.302*(1) ±0.7	22.75(3) ±0.20	−95.362(2) ±0.205
Talc	−1320.412 (1) ±0.9	62.34(3) ±0.15	−304.272(2) ±0.165
Water	−56.688 (3) ±0.020	16.71(3) ±0.03	−38.996(2) ±0.031
Quartz	−204.646 (3) ±0.410	9.88(3) ±0.02	−43.616(2) ±0.143
Antigorite	−928.756†(2) ±1.1	53.2 (4) ±0.5	−246.726(2) ±0.503
Enstatite	−348.955 (2) ±0.6	16.22(3) ±0.10	−69.584(2) ±0.106
Anthophyllite	−2711.321 (2) ±1.7	133.62(9) ±0.32	−576.210(2) ±0.335
Oxygen	—	—	—
Hydrogen	—	—	—

* Pure, synthetic forsterite, −491.435 ± 0.7 kcal/gf.
** $Cp = a + b\ 10^{-3} + c\ 10^5\ T^{-2}$ (Kelley, 1960).
† Based on $Mg_{2.825}Si_2O_5(OH)_{3.65}$ (Kunze, 1956), −966.728 kcal/gf based on $Mg_3Si_2O_5(OH)_4$.
†† Values above 848 K.
Sources:
(1) Hemley and others (1977).
(2) Proposed or calculated in this study; S°_f values are calculated from the S° values of the compounds and the elements listed in Robie and Waldbaum (1968).

of the Al (calculated as Mg) to tetrahedral coordination. Similar compositions are illustrated by Faust and Fahey (1962).

Sepiolite is a relatively rare mineral in the MgO–SiO_2–H_2O system and represents the highest Si/Mg ratio. A mineral of similar structure, but typically containing appreciably more aluminum, is attapulgite or palygorskite. Sepiolite dissolution, which is nonstoichiometric, was studied by Christ, Hostetler, and Seibert (1973) and its synthesis by Wollast, Mackenzie, and Bricker (1968). Singer and Norrish (1974) have investigated palygorskite. Sepiolite has variable water content, but the composition may be idealized as $Mg_2Si_3O_{7.5}(OH) \cdot 3H_2O$. From the free energy of formation given by Christ, Hostetler, and Seibert (−1105.560 kcal/gf), the talc–sepiolite boundary at 298, 1 bar, is at log $mSiO_2$ = 3.71, a very high value. Sepiolite therefore appears to be metastable relative to quartz plus either talc or Mg–montmorillonite, even though its synthesis at low temperatures is fairly easily demonstrated. This transformation, in fact, may be incipiently underway in the experiments of Christ, Hostetler, and Seibert as the aqueous composition at 90°C for a well-crystallized sepiolite plots within the talc field on the metastable sepiolite boundary and essentially on the 1-bar solubility curve for quartz.

The environment of formation of sepiolite has been summarized by Wollast, Mackenzie, and Bricker. An unusually high aqueous silica activity is obviously appropriate, but a moderate silica activity coupled with a high $[Mg^{+2}]/[H^+]^2$ value (for example, high pH) would also

Thermochemical values used [25°C, 1 bar, except as noted]

V (cal/bar gf)	Cp** a	b	c	
1.0466 (3) ±0.0007	35.81	6.54	−8.52(4)	Forsterite
3.2564 (3) ±0.0047	84.58	41.68	−17.96(7)	Talc
0.4219 (3) ±0.00007	—	—	—	Water
0.54226(3) ±0.00002	14.41 11.22	1.94†† 8.20	— −2.70(9)	Quartz
2.499 (5) ±0.007	75.82	31.6	−17.58(4)	Antigorite
0.75215(3) ±0.0012	24.55	4.74	−6.28(8)	Enstatite
6.3207 (6)	196.32	43.52	46.96(8)	Anthophyllite
—	7.16	1.00	−0.4 (8)	Oxygen
—	6.52	0.78	0.12(8)	Hydrogen

(3) Robie and Waldbaum (1968).
(4) King and others (1967).
(5) Calculated from data of Page and Coleman (1967).
(6) Zen (1971).
(7) Robie (personal commun.).
(8) Kelley (1960).
(9) Mel'nik and Onoprienko (1969).

suffice for metastable formation within the talc or chrysotile fields (see fig. 9). This latter type of chemical environment is no doubt the type responsible for the occasional formation of sepiolite during serpentinization of mafic rocks. This also would apply to the formation of sepiolite or palygorskite in some saline lakes and evaporating soil waters. An aqueous environment low in Al and Fe but quite high in $[Mg^{+2}]/[H^+]^2$ is apparently necessary and adequate to preclude formation of a layer silicate such as montmorillonite, judging from the work of Singer and Norrish (1974).

Sepiolite is also occasionally found as fracture fillings and coatings on fault surfaces in carbonate rocks and silicated carbonate rocks (for example, diopside) in some mining districts (W. W. Atkinson, personal commun.). These occurrences apparently represent the products of spent solutions of hydrothermal alteration or hot spring activity, characterized by high aqueous silica activity (opal is sometimes present) and relatively high $[Mg^{2+}]/[H^+]^2$ ratio.

Additional low-temperature mineral species exist in the MgO–SiO_2–H_2O system (see Brown, 1961; Deer, Howie, and Zussman, 1962), but their aqueous equilibria and thermochemical relations have not been worked out. Lizardite is a serpentine phase commonly associated as a matrix with coarser chrysotile. It also tends to show higher Fe and Al contents than chrysotile and has a platy rather than tubular morphology. Chrysotile and lizardite are more abundant than antigorite in serpentinites,

except in metamorphic terranes. Stevensite is the end-member montmorillonite for the system, having an essentially hydrated talc composition. Whether the hypothetical end-member is stable relative to talc is questionable, even at Earth-surface temperatures, but saponite (the impure Al, Fe-bearing equilivalent) is of common occurrence and might well be stable. The position of the saponite–serpentine and saponite–talc aqueous silica and cation ratio equilibrium boundaries are important questions relating to weathering and hydrothermal alteration.

STABILITY OF ANTHOPHYLLITE AND ENSTATITE

Relationships at 1 kb.—The important consideration at high temperatures in the MgO–SiO_2–H_2O system is the stability relations of anthophyllite, talc, enstatite, and forsterite. An extensive experimental study on anthophyllite synthesis and stability was presented by Greenwood (1963), and one of the earlier discussions of petrogenetic relationships was given by Korzhinsky (1962). Compositions and X-ray data for the phases used in the present investigation are given in table 1. Natural anthophyllite, natural and synthetic talc and enstatite, and synthetic forsterite were used in the study. For the equilibration runs recorded in table 2 and figure 2, the data correspond to the use of the exchanged natural anthophyllite and enstatite, natural talc, and synthetic forsterite of table 1. No systematic differences were noted in the use of natural versus synthetic or exchanged versus unexchanged materials, but the data were not sufficiently numerous for full evaluation of this question. Anthophyllite and enstatite were exchanged by hydrothermal treatment, using 1 m $MgCl_2$ at 720°C and 2 kb. Relatively pure Mg minerals were thus produced, and any traces of talc contamination, which were evident in the enstatite, were also eliminated.

The experimental results, on an expanded scale, are given in figure 2. The quartz solubility shown is based on a continuation of the lower temperature studies reported in the preceding paper (Hemley and others, 1977). The field boundaries correspond to silication-desilication reactions (reactions 9-13), and their intercepts correspond to isobaric dehydration reactions. These intercepts are at 636° ± 7°C (talc–forsterite–anthophyllite), 670° ± 7°C (anthophyllite–forsterite–enstatite), 643° ± 8°C (talc–forsterite–enstatite), 675° ± 7°C (talc–anthophyllite–quartz), and 690° ± 8°C (talc–enstatite–quartz). The anthophyllite–enstatite–quartz point was not determined, but a temperature of 729°C is indicated from the derived thermodynamic relations. The dehydration reactions corresponding to the 1 kb invariant points are as follows:

$$4 \text{ forsterite} + 9 \text{ talc} = 5 \text{ anthophyllite} + 4\ H_2O \quad (3)$$

$$7 \text{ talc} = 3 \text{ anthophyllite} + 4 \text{ quartz} + 4\ H_2O \quad (4)$$

$$\text{anthophyllite} + \text{forsterite} = 9 \text{ enstatite} + H_2O \quad (5)$$

$$\text{anthophyllite} = 7 \text{ enstatite} + \text{quartz} + H_2O \quad (6)$$

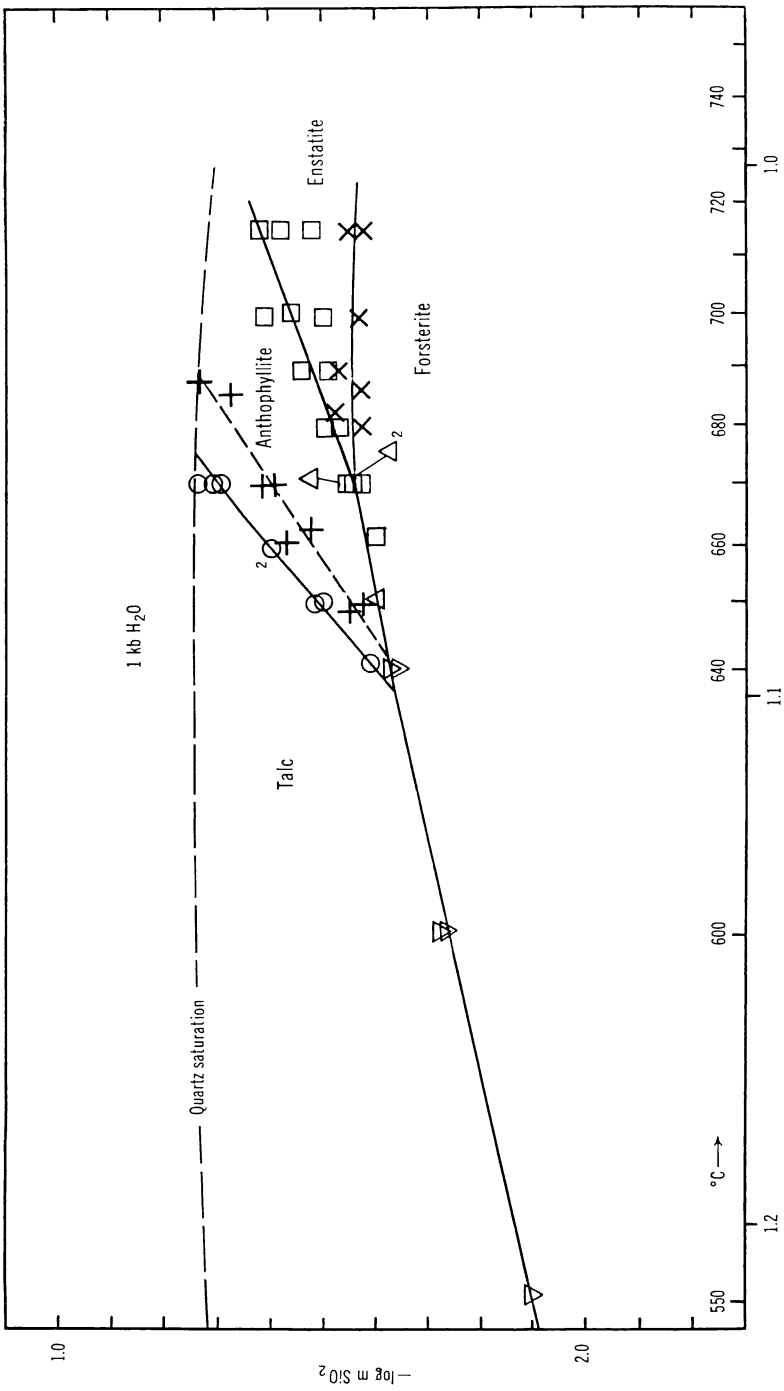

Fig. 2. Anthophyllite stability relations at 1 kb H_2O. O, talc–anthophyllite; +, talc–enstatite; □, anthophyllite–enstatite; △, anthophyllite–forsterite; X, enstatite–forsterite; ▽, talc–forsterite.

$$\text{talc} + \text{forsterite} = 5\ \text{enstatite} + H_2O \quad (7)$$

$$\text{talc} = 3\ \text{enstatite} + \text{quartz} + H_2O \quad (8)$$

The precision stated for the above reaction points is better than that assigned in an earlier report (Hemley and others, 1975), although the topological relations outlined remained unchanged. The reason for the greater scatter in the experimental data toward the high-temperature end of the anthophyllite–enstatite boundary is not clear, but the low-temperature intercept with the forsterite field is well defined.

Gibbs free energies of formation for anthophyllite were calculated from the intercepts on the talc–anthophyllite equilibrium curve. These are −2711.053 and −2711.589 kcal/gf at the forsterite and quartz intercepts, respectively. The mean value of −2711.321 ± 1.7 kcal/gf is entered in table 3. The $G°_{f,298}$ for pure, synthetic forsterite was used in the calculations. Satisfactory entropy and heat-capacity data for anthophyllite are not yet available. The entropy value is from Mel'nik and Onoprienko (1969), based on the work of Greenwood (1963). It differs very little (0.1 entropy units higher) from the value obtained by oxide summation, using the Latimer (1952) value of 9.4 entropy units for bound H_2O. The heat-capacity constants are from Kelley (1960), reported as $MgSiO_3$ (amphibole-type). This value results in greater internal consistency among the equilibria than a value proposed by Mel'nik and Onoprienko.

The Gibbs free energy for enstatite was then computed from the forsterite–anthophyllite–enstatite intercept, using the above average anthophyllite value and the entropy and heat-capacity data for clinoenstatite (Robie and Waldbaum, 1968). The value is −348.955 ± 0.6 kcal/gf and is entered in table 3. It is intermediate between enstatite values obtained from the metastable talc–enstatite curve, −348.936 and −349.004 kcal/gf at the forsterite and quartz intercepts, respectively. The agreement between the various anthophyllite and enstatite free energy values is satisfactory and, in fact, remarkably good in view of the uncertainties in the current entropy and heat-capacity information.

The foregoing experimental results show lower reaction temperatures than the corresponding values of Greenwood (1963). However, his 1 kb data are not nearly as extensive as his information at higher pressure and perhaps should not be used for rigorous comparison. They will not be discussed further, therefore, except to note that contaminants such as clinoenstatite and cristobalite were present in the synthetic material used by Greenwood. These could have resulted in the formation of anthophyllite under PT conditions, where anthophyllite should not be stable. The synthesis of pure anthophyllite is a most difficult task and was not attempted in the present study.

The growth of anthophyllite from talc plus enstatite within its field of stability in figure 2 was observed. This observation tends to contradict the interesting suggestion of Zen (1971) that pure Mg–anthophyllite may be unstable relative to talc plus enstatite, requiring minor iron substitu-

tion for its stabilization. The presence of Fe theoretically should enlarge the field of stability of anthophyllite somewhat relative to the pure mineral as discussed by Evans and Trommsdorf (1974), but an experimental assessment of this problem was not attempted. Calculations on the enstatite–anthophyllite equilibrium, using the mineral analyses of table 1 and assuming ideal solid solution for the Mg and Fe amphibole end-members, indicate only a small decrease in the anthophyllite field for pure Mg–anthophyllite. The anthophyllite field is essentially at its minimum size.

These experimental results are in good agreement with the studies of Chernosky (1974) on enstatite. Chernosky reported 638° ± 5°C for talc–forsterite–enstatite and 697° ± 5°C for talc–enstatite–quartz, using conventional hydrothermal methods.

Relationships at other pressures and their implications.—Experimentation was extended in this study to confining pressures other than 1 kb in only a few runs. The changes that should occur, however, can be understood readily from a qualitative consideration of the effect of pressure on the specific reactions.

Consider the following five equilibria relating to the anthophyllite field in figures 1 and 2:

$$2 \text{ talc} + 8\ H_2O = 3 \text{ forsterite} + 5\ H_4SiO_4 \qquad K = \frac{[H_4SiO_4]}{[H_2O]^{1.6}} \qquad (9)$$

$$7 \text{ talc} + 4\ H_2O = 3 \text{ anthophyllite} + 4\ H_4SiO_4 \qquad K = \frac{[H_4SiO_4]}{[H_2O]} \qquad (10)$$

$$\text{anthophyllite} + H_2O = 7 \text{ enstatite} + H_4SiO_4 \qquad K = \frac{[H_4SiO_4]}{[H_2O]} \qquad (11)$$

$$2 \text{ enstatite} + 2\ H_2O = \text{forsterite} + H_4SiO_4 \qquad K = \frac{[H_4SiO_4]}{[H_2O]^2} \qquad (12)$$

$$2 \text{ anthophyllite} + 16\ H_2O = \text{forsterite} + 9\ H_4SiO_4 \qquad K = \frac{[H_4SiO_4]}{[H_2O]^{1.8}} \qquad (13)$$

including the quartz-solubility reaction

$$\text{quartz} + 2\ H_2O = H_4SiO_4 \qquad K = \frac{[H_4SiO_4]}{[H_2O]^2} \qquad (14)$$

It is apparent that the reaction defining the bottom of the anthophyllite field in figure 2, reaction (13), has greater dependence on fugacity of H_2O than the two side boundaries, reactions (10) and (11). Thus, when f_{H_2O} increases, the forsterite–anthophyllite boundary moves relatively higher on the anthophyllite field, and the field widens. Conversely, the field narrows at lower water pressures. The dissolution reaction for quartz is slightly more sensitive to f_{H_2O} than the anthophyllite–forsterite reaction; therefore, the quartz curve migrates on the diagram at a slightly faster rate.

Although the foregoing discussion is concerned only with P_{H_2O}, the implied trends in the equilibria remain substantially the same when incorporating the smaller $P\Delta V$ effect for the other constituents of the reaction. The absolute displacement of the phase boundaries with change in P_{H_2O} cannot be calculated from the equilibrium expressions without such corrections, including the pressure effect on activity coefficients of aqueous constituents, although this latter effect is generally relatively insignificant. A few experimental data on the anthophyllite boundaries at 2 kb $P_{total} = P_{H_2O}$ are illustrated in figure 3. The runs were only in the direction of silica dissolution, and equilibrium was not demonstrated. However, the anthophyllite field has expanded, and, because dissolution equilibrium was not fully attained, the field should be even more enlarged than indicated.

The foregoing considerations emphasize that the Q-absent invariant point (Q) corresponding to the convergence of talc, enstatite, forsterite, and anthophyllite in figure 2 can be attained only at lower P_{H_2O}. Similarly, the (F) invariant point, corresponding to talc–enstatite–anthophyllite–quartz–water, requires an even lower P_{H_2O} for its realization. The trends indicated by the present work are illustrated schematically in figure 4A as log $mSiO_2$ versus 1/T plots, stepwise with decreasing pressure.

The related pressure-temperature plot is shown in figure 5. These are calculated curves (100 bars to 4 kb), based upon the data of table 3. The average anthophyllite and enstatite free energy values given in the table apparently tend to compensate for errors arising from inadequate heat capacity data or other sources, inasmuch as the curves are brought into very close convergence at their respective invariant points (better seen on a large scale) using these values. Some of the calculated curves show temperatures at 1 kb slightly different from their experimental values. The differences are within the estimated experimental uncertainty in all cases, except for talc–forsterite–anthophyllite, which is shifted about 9° lower to 627°C. The calculated curves for the metastable en-

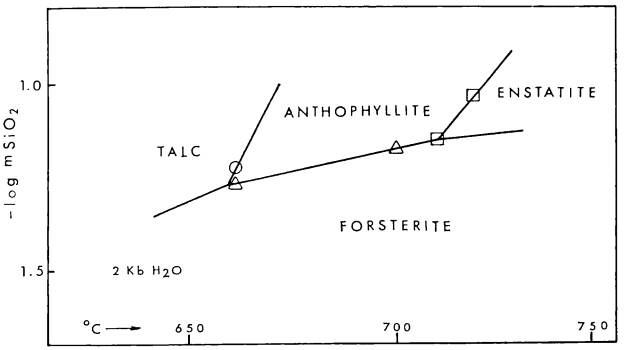

Fig. 3. Experimental data on anthophyllite relationships showing expansion of its field at 2 kb H_2O. Same symbols as figure 2.

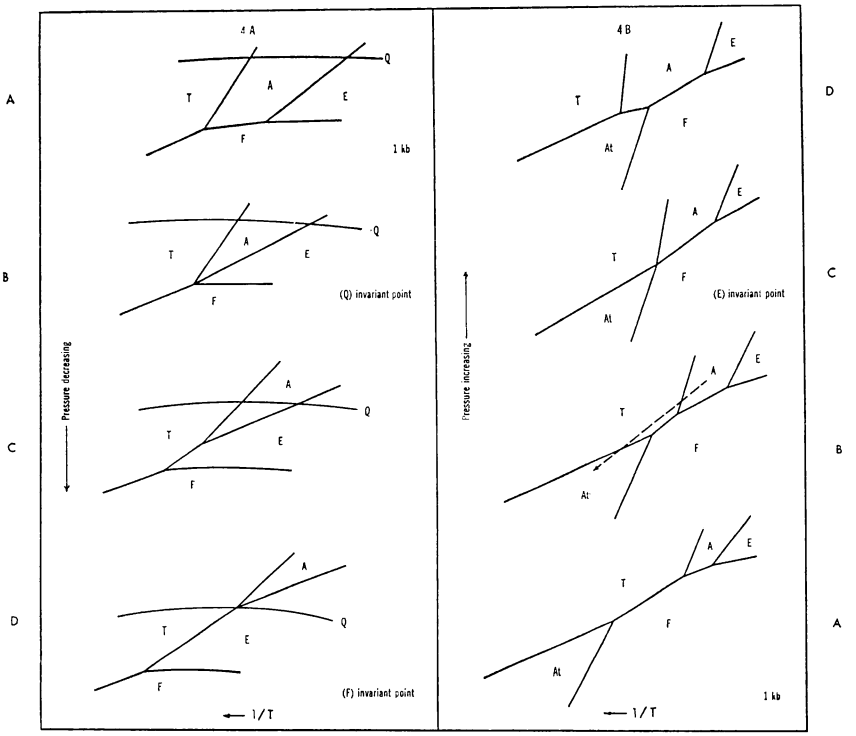

Fig. 4. A and B. Schematic stability relations, log $mSiO_2$ versus $1/T$ as a function of pressure, $P_{total} = P_{H_2O}$. Symbols: T, talc; A, anthophyllite; E, enstatite; F, forsterite; Q, quartz; At, antigorite. The remaining phases in the system at the invariant points are not listed. The dashed arrow in (4B) is discussed in text.

statite assemblages are in nearly exact agreement with the results of Chernosky (1974). The calculated values are preferred values inasmuch as they represent complete thermochemical consistency for the data, but the possible sources of error in the thermochemical calculations should also be kept in mind.

As already noted in the discussion and shown by the dashed talc–enstatite desilication curve in figure 2, the talc–forsterite–enstatite and talc–enstatite–quartz dehydration reactions are low pressure changes, metastable at 1 kb. The slope of the H_2O-independent reaction,

$$\text{talc} + 4 \text{ enstatite} = \text{anthophyllite} \qquad (15)$$

is 115 bars/degree on the basis of the data of table 3 and is probably not greatly in error. The curve flattens somewhat at higher pressure, but adequate compressibility data are not yet available for accurate calculation. The (Q) and (F) invariant points are at approx 602°C and 500 ± 100 and 175 ± 50 bars, respectively. The association talc–enstatite is stable only within the relatively low P_{H_2O} range indicated between (Q) and (F) (at higher P_{H_2O} the pair will convert to talc–forsterite, and at

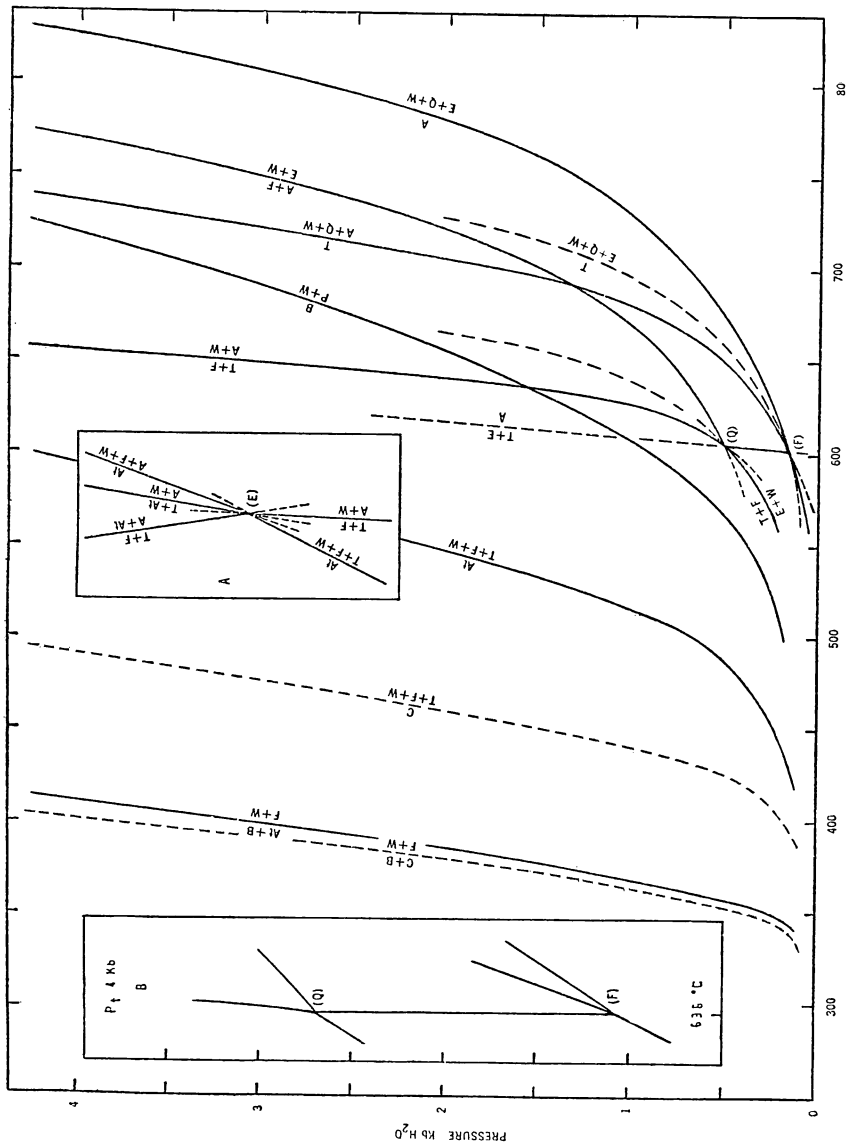

Fig. 5. Calculated pressure-temperature curves for the system MgO–SiO_2–H_2O, based on 1 kb experimental stability data and derived thermodynamic relations. Symbols: T, talc; A, anthophyllite; E, enstatite; F, forsterite; Q, quartz; At, antigorite; B, brucite; P, periclase. Inset A shows an additional invariant point for very high pressure. Inset B shows the position of invariant points (Q) and (F) at $P_{total} = 4$ kb. As discussed in text, p. 377, chrysotile appears to be stable at low temperatures but metastable with respect to antigorite in the portion of the figure shown.

lower P_{H_2O} to enstatite–quartz). However, a high total pressure raises the P_{H_2O} range, as discussed in a later paragraph, and brings the talc–enstatite assemblage into a geologically less restricted region of stability. It is apparent that the total pressures required are geologically reasonable. Distinct from the invariant points, the two indifferent crossings shown in figure 5 do not, of course, correspond to points where a larger number of phases coexist at equilibrium. The PT net expressed in figure 5 and required by the experimental relationships differs considerably from that given by Greenwood (1963) and used by Chernosky (1974) and Zen and Chernosky (1976).

Deductions similar to the above on the high-temperature phase relations in this system can also be made concerning the low-temperature assemblages in this system. The following reactions are of interest, serpentine signifying either chrysotile or antigorite:

$$\text{talc} + 5\ H_2O = \text{serpentine} + 2\ H_4SiO_4, \qquad K = \frac{[H_4SiO_4]}{[H_2O]^{2.5}} \tag{16}$$

$$2\ \text{talc} + 8\ H_2O = 3\ \text{forsterite} + 5\ H_4SiO_4, \qquad K = \frac{[H_4SiO_4]}{[H_2O]^{1.6}} \tag{17}$$

$$\text{serpentine} + 5\ H_2O = 3\ \text{brucite} + 2\ H_4SiO_4, \qquad K = \frac{[H_4SiO_4]}{[H_2O]^{2.5}} \tag{18}$$

$$2\ \text{serpentine} = 3\ \text{forsterite} + H_4SiO_4 + 2\ H_2O, \qquad K = [H_4SiO_4]\,[H_2O]^2. \tag{19}$$

It is seen that the talc–serpentine and serpentine–brucite reactions show the same H_4SiO_4 variation with respect to fugacity of H_2O. Because of this fact and their relatively large separation in H_4SiO_4 activity on the diagram (fig. 1), it would be virtually impossible for convergence of the two equilibria to occur at any pressure. The ΔV of the solids for the two reactions are very similar and would have an insignificant effect on the relationships. The invariant point at which talc and brucite coexist, that is, the serpentine–talc–forsterite–brucite–water invariant point, therefore, cannot be attained in the stable system.

It will be noted, however, that the talc–serpentine reaction is more f_{H_2O} sensitive than the talc–forsterite and anthophyllite–forsterite reactions. In this higher temperature context, antigorite is the more appropriate serpentine phase to consider. When P_{H_2O} increases, antigorite will therefore encroach upon forsterite and should eventually reach the anthophyllite field. The result is an invariant point representing the assemblage talc–antigorite–anthophyllite–forsterite–water. Calculations indicate that it will occur only at very high pressure (above 10 kb), however; therefore, it is of limited geological significance. These changes are illustrated diagrammatically in figure 4B, with stepwise increase in pressure. The invariant point is illustrated in the small inset of figure 5. At a still higher pressure, antigorite and anthophyllite develop a common boundary. The curves for quartz and forsterite-enstatite migrate at essen-

tially the same rate on the diagram as P_{H_2O} changes, and therefore quartz and forsterite should remain incompatible.

The importance of considering chemical equilibria other than dehydration and H_2O-independent reactions in establishing the overall PT relationships for a system should be clear from the foregoing analysis involving the aqueous silica dependent relationships. By using this approach, a broader and more definitive basis is developed for evaluating reactions and eliminating various equilibria and invariant points from consideration.

Relationships at $P_{total} > P_{H_2O}$ are also of interest geologically and are illustrated in the large inset of figure 5. Such pressure relationships might be the result of either high intergranular rock pressure or the presence of other gaseous components, CO_2 being of particular importance in this system. Volume changes exclusive of H_2O determine the displacement of the silica dissolution and thermal dehydration reactions under these conditions. Referring to the several dehydration reactions shown in figure 5, the reactions have a negative ΔV_s, and the curves are therefore displaced to lower temperatures by an increase in total pressure. In addition to allowing dehydration to occur at a lower temperature, the result is to shift the intersection with the H_2O-independent talc–enstatite–anthophyllite curve (which remains fixed) to a higher P_{H_2O} value and to modify the position of the invariant points. At a total pressure of 4 kb, for example, the stability of the talc–enstatite–anthophyllite assemblage extends to approx 636°C, as extrapolated from the curve in figure 5. The intercept of the talc–forsterite–anthophyllite–water and forsterite–anthophyllite–enstatite–water curves (point Q) will also occur at a P_{total} of 4 kb at this temperature, but the P_{H_2O} value of the intercept will be approx 2.7 kb[1]. Similarly, the (F) point can also exist at 4 kb total pressure, but only if P_{H_2O} is approx 1.1 kb. Increasing P_{total} relative to P_{H_2O} thus raises the P_{H_2O} values of the (Q) and (F) invariant points but does not produce additional invariant points or change the topology of the diagram.

SOME GEOLOGIC APPLICATIONS

The PT grid, together with T-activity or 1/T-activity plots, constitute useful tools for geologic analysis. The PT grid outlines the total physical framework for metamorphism, whereas the 1/T-activity plots depict the controls on metasomatism within that framework. Metasomatism may range from minor, as in a typical hornfels, to major, as in a skarn. Extensive metasomatism does not invalidate a pressure-temperature approach to the systematization of metamorphic assemblages but obviously does emphasize additional reactions that must be considered for a full understanding of the genetic process. The limitations in applying

[1] This is calculated from the relation $(P_{total} - P_{H_2O\ equil})\ \Delta V_s = -G^*_{H_2O\ unknown} + G^*_{H_2O\ equil}$ at a given temperature, using the tables of Fisher and Zen (1971). The subscript equil refers to values along any given reaction curve of figure 5. No correction has been made for compressibility and thermal expansion of the solids. The entire PT net may be recalculated in this manner.

experimental data from a pure or restricted system to geologic problems should, of course, be realized (for example, the role of Fe in anthophyllite, as noted earlier), but generalized relations, such as those discussed below, would still be valid.

Contact metamorphism and metasomatism.—The changes produced by varying temperature and aqueous silica concentration or activity[2] in figure 1 are clear. For example, by increasing temperature at constant aqueous silica concentration, one may traverse successively from talc to serpentine to forsterite or talc to anthophyllite to enstatite, reflecting the increasing tendency of the phases to lose silica to the solution as temperature increases. Increasing aqueous silica concentration on the diagram results, of course, in phases of higher silica content. Intrusion of an ultramafic body into a quartz-bearing environment, for example, would tend to produce assemblages lying between the quartz saturation curve and the forsterite field of figure 1. One might also note, however, that, at constant or even decreasing aqueous silica concentration, but accompanied by decreasing temperature, a zonation to higher silica phases (enstatite to anthophyllite to talc, or forsterite to talc) is possible from the relations shown in figure 1. This is the path for rock alteration. Such changes, added to the pattern of appropriate thermal dehydration reactions as given in figure 5, would also be expected outward from a hot intrusive body in mafic rocks, for example, in the contact metamorphism of serpentinite. This is not to say that the observed mineral zonation pattern would be the product of metasomatic processes, but that such processes, to the extent that they occur, would operate consistently within the requirements of the PT environment. For example, any addition of silica to the host rocks by the intrusive would be manifested as an increase in abundance of the more silica-rich phase or phases in the contact assemblage, for example, more anthophyllite in the anthophyllite–forsterite assemblage, but the zonation from higher-Mg phases near the contact to higher-Si phases farther out would be maintained. Such a contact metamorphic pattern has been described, for example, by Trommsdorf and Evans (1972) and by Frost (1975). A full understanding of a given metamorphic process depends, of course, upon detailed documentation of change in bulk composition relative to that of the original rock, and unfortunately this ordinarily poses a difficult and tedious sampling problem.

Finally, even with no introduction of new material into the environment by the intrusive, metasomatic effects could be expected within the aureole simply as a consequence of a temperature gradient, a migrating pore-fluid phase, and the relationships shown in figure 1. Silica dissolution in hotter regions of the intrusive or aureole and silica fixation in relatively cooler regions would be the result. Such transfer and redistribution of material within a given defined system might more descriptively be

[2] The standard state is the hypothetical, ideal 1 m solution at the temperature and pressure of interest.

termed *endometasomatism*. In this system, talc veining and alteration would be the most common manifestation of silica fixation, but the formation of anthophyllite, and even of the assemblage talc–enstatite, could be expected under the appropriate PT conditions.

The relationships of figures 1, 4, and 5 apply, for example, to the interesting metamorphic alteration patterns described by Frost (1975) and Evans and Trommsdorf (1974). These will be summarized only briefly. The pattern from Frost indicates later, cooler SiO_2 and H_2O fixation in an enstatite–forsterite host rock to form talc–enstatite veins. The veins locally show talc centers. The pattern described by Evans and Trommsdorf consists of talc–enstatite–magnesite veins, with anthophyllite centers, formed from a talc–forsterite host rock. In this example, silication resulted from the fixation of CO_2 to form magnesite, with the silica released then consumed in silica-fixation reactions. Silication within the stability field of talc–forsterite, however, would produce only talc, and, therefore, a lower P_{H_2O} (coupled with a higher P_{CO_2} as is required for fixation of the CO_2) is indicated for the environment of the host structures. Temperatures may also have been somewhat higher in that environment. Enstatite is prominent and would be favored in the assemblage by silication at P_{H_2O} values barely high enough to sustain the formation of talc. Thus, for both these patterns, the conditions indicated correspond to an environment on and near the TFEW curve at the bottom of figure 5 or on the same curve in a diagram such as inset 5B. The corresponding point in figure 4A(C) is the talc–forsterite–enstatite isobaric invariant point (the migration of this point with change in P_{H_2O} generates the TFEW curve of fig. 5).

The eventual elimination of forsterite from the vein assemblage corresponds to relative movement upward and away from the isobaric invariant point in figure 4A(C). With increase in temperature, movement is upward along the buffered TE boundary, and with sufficient rise in temperature, the anthophyllite field is reached. Although increasing temperature is not completely ruled out on geologic grounds for the origin of the anthophyllite, an essentially isothermal process is certainly more likely. As discussed by Evans and Trommsdorf, later altering solutions may have increased in Fe activity relative to Mg, thereby enlarging the field of anthophyllite relative to talc–enstatite and expanding it downward. Finally, although neither an increase nor decrease in P_{H_2O} at constant P_{total} would produce anthophyllite, a decrease in P_{total} at constant temperature would tend to have such an effect. Note that the temperature specified in inset 5B would be lower at a lower P_{total}. This last alternative is perhaps the most plausible genetic interpretation, as a drop in P_{total} for the system may well have occurred during the time of later tectonism. A late set of anthophyllite veins that crosscut the composite veins is also present.

Returning to the general problem, metasomatic changes should often be produced or accentuated by a convective pore-fluid or groundwater

phase mobilized by the heat source implicit in magmatic intrusion. Such a process would not necessarily develop early following intrusion, as it would depend upon access of water and the total pressure conditions relative to hydrostatic head (Gustafson and Hunt, 1975), but the effects are probably of importance even in fairly deep-seated intrusive processes. The importance with respect to isotope exchange is well established. This accession of magmatic volatiles, when and where it occurs, produces, of course, an added metasomatic imprint.

Metasomatic relations under isothermal-isobaric conditions are more readily analyzed in terms of the individual reactions relating two minerals, such as (20) below, or in terms of activity-activity diagrams for polyphase assemblages. In constructing such diagrams, care should be taken to write the reactions in terms of the appropriate aqueous species present in solution, to the extent that they are known. As noted earlier (Hemley and others, 1977), the evaluation of the net free energy change of a reaction at constant temperature and pressure is independent of the formula assumed for an aqueous complex, whether that of silica or any other dissolved constituent, because water cancels out of the reaction. In evaluating the relative roles of water activity (hence P_{H_2O}) and aqueous silica activity in controlling a reaction in which both are involved, however, this indifference no longer holds, and an effort must be made to represent the true reaction involved. This applies to both homogeneous and heterogeneous equilibria.

Consider, for example, the assemblage talc–antigorite–anthophyllite. This assemblage was discussed in a previous paragraph as a possible, though geologically improbable, high P_{H_2O} association in this system. If we neglect the slightly higher Si content of antigorite, the dissolution reactions are:

$$\text{talc} + 5\ H_2O = \text{antigorite} + 2\ H_4SiO_4, \qquad K = \frac{[H_4SiO_4]}{[H_2O]^{2.5}} \tag{20}$$

$$7\ \text{talc} + 4\ H_2O = 3\ \text{anthophyllite} + 4\ H_4SiO_4, \qquad K = \frac{[H_4SiO_4]}{[H_2O]} \tag{21}$$

$$3\ \text{anthophyllite} + 31\ H_2O = 7\ \text{antigorite} + 10\ H_4SiO_4, \qquad K = \frac{[H_4SiO_4]}{[H_2O]^{3.1}} \tag{22}$$

Figure 6 is the corresponding activity-activity diagram, based on the slopes given in the above equilibrium expressions. If a greater degree of hydration is assumed for aqueous silica, the anthophyllite field becomes narrower, but the signs of the slopes remain the same. As pointed out in the preceding paper (Hemley and others, 1977), H_4SiO_4 is used in the present study as an adequate, approx representation of the silica speciation involved, but the possible importance of higher hydration, such as $H_4SiO_4 \cdot 2H_2O$ or $SiO_2 \cdot 4H_2O$, is indicated from other work (Crerar and Anderson, 1971).

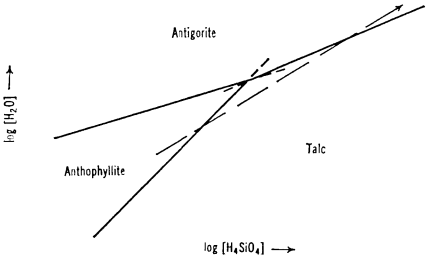

Fig. 6. Schematic of anthophyllite–antigorite–talc stability relations at constant temperature and pressure.

In the conventional petrological procedure for writing such reactions, speciation is generally ignored and aqueous silica is represented simply as the dissolved, unassociated oxide. The state of the participants of a reaction must be clear to have valid chemical meaning. Expressing the state of the silica unambiguously as aqueous anhydrous, we have:

$$\text{talc} + H_2O = \text{antigorite} + 2\ SiO_{2\ aq\ anhy} \tag{20A}$$

$$7\ \text{talc} = 3\ \text{anthophyllite} + 4\ SiO_{2\ aq\ anhy} + 4\ H_2O \tag{21A}$$

$$3\ \text{anthophyllite} + 11\ H_2O = 7\ \text{antigorite} + 10\ SiO_{2\ aq\ anhy} \tag{22A}$$

The two sets of equations are then related through the reaction $2H_2O + SiO_{2\ aq\ anhy} = H_4SiO_4$.

The two sets of reactions are obviously not equivalent views or expressions of the same equilibria. The hydration reaction shown is displaced strongly to the right with the hypothetical, anhydrous, aqueous silica reduced to very low concentrations, if, indeed, it exists as an aqueous species under any PT conditions of interest. A chemical potential or activity diagram based upon the second set of equilibria, therefore, does not apply to the dominant or significant aqueous silica relationships of the system.

On the other hand, if eqs 20A through 22A are written with hydration of silica implicitly assumed but considered unnecessary to express, as is perhaps the usual intent, the slopes in the resulting $\mu SiO_2 - \mu H_2O$ diagram are all more or less in error. The error is most serious for reaction 21A, in which water and silica are depicted on the same side of the reaction and therefore are inversely related. This violates experiment, in which it is clear that increasing P_{H_2O} on the talc–anthophyllite assemblage produces anthophyllite and increases, not decreases, aqueous silica in solution. Eq 21A, written in such a manner, would not be representative of the true reaction, therefore, and diagrams based upon it would not be representative of a geologic process involving that reaction. Aqueous speciation is unavoidably an important consideration in petrologic processes, just as it is in the rather similar field of chemical engineering processes and practice.

The anthophyllite-bearing rocks of southeastern Pennsylvania and northeastern Maryland consist dominantly of associations of anthophyl-

lite, talc, and serpentine (antigorite). Outward from associated albitite dikes, consecutive zones of anthophyllite, talc, and serpentine are observed (Larsen, 1928), anthophyllite and serpentine never being in contact. As seen by the arrow in figure 6, such a relationship would be produced isothermally by an upward gradient in both aqueous silica and H_2O activity. On the basis of the diagram drawn from eqs 20A through 22A, however, a gradient exclusively in H_2O activity could be proposed as a possible explanation for the zonal relationships (Greenwood, 1963).

The alternative mode of origin, also discussed by Greenwood, is nonisothermal. The anthophyllite-bearing assemblages are associated with intrusive acidic dikes, and these were presumably responsible for the thermal and chemical environment of metasomatism. For this interpretation, one could refer to figure 1 or to sketch B of figure 4B. The dashed arrow represents a decreasing gradient in both temperature and aqueous silica concentration, at a more or less constant P_{H_2O}, from the field of anthophyllite (associated with the dike) to the serpentine (host rock). This is the more plausible genetic interpretation, as it is unlikely that a gradient of increasing silica activity would occur outward into the very low silica serpentine (or original mafic) country rock.

The foregoing example should not be considered an isolated or unusual case in geology. Reactions relating the phases pyrophyllite, kaolinite, and andalusite are analogous to those just discussed, with the relationship between pyrophyllite and an Al_2SiO_5 phase analogous to reaction (21). Again, completely different geologic relationships are implied by chemical potential diagrams drawn up in the contrasting manners. Equilibria in the Al_2O_3–SiO_2–H_2O system will be discussed in a later paper.

Isochemical cooling and reaction.—The foregoing discussion has dealt with the application of temperature-activity and activity-activity diagrams to problems of metasomatism in this system. Controls impressed upon and external to the system are implicitly assumed for such processes that produce changes in bulk chemical composition.

A contrasting and equally important consideration is chemical change within the system along isochemical heating or cooling paths. Externally controlled chemical potentials do not then govern reactions, and the solid phases buffer the system. P_{H_2O} might be externally controlled but is probably variable in magnitude. The resulting changes have their most obvious application to igneous and metamorphic retrograde processes.

Commencing with the enstatite–forsterite pair at high temperature (a harzburgite peridotite) and assuming a finite P_{H_2O} appropriate to the relations of figure 1, the assemblage will cool with consumption of aqueous silica and production of H_2O (reaction 12 reversed), until the forsterite–enstatite–anthophyllite isobaric invariant point is reached. Here enstatite will convert to anthophyllite–forsterite at constant aqueous SiO_2 concentration and temperature (reaction 5 reversed), until either H_2O or enstatite is entirely consumed. If H_2O is depleted, reaction, of course,

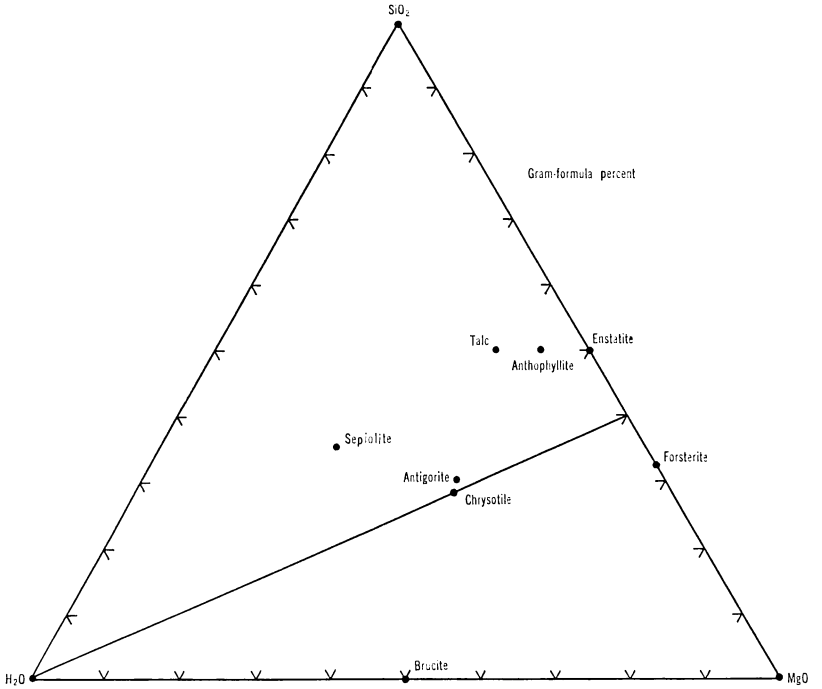

Fig. 7. Composition diagram for the system MgO–SiO_2–H_2O. The composition of antigorite is from Kunze (1956) and of sepiolite from Christ, Hostetler, and Seibert (1973).

ceases. If enstatite disappears, further cooling consumes silica (reaction 13 reversed) and progresses to the anthophyllite–forsterite–talc intercept where the same type of process is repeated, anthophyllite being destroyed (reaction 3 reversed). The resulting talc–forsterite assemblage then follows the talc-forsterite boundary (reaction 9 reversed) to the talc–forsterite–antigorite intercept. At this point, the system will take different paths, depending upon bulk composition. As seen from the relationships in figure 7, if the original forsterite–enstatite proportions in the rock are on the high-silica side of serpentine (a high-enstatite rock), the path will proceed along the talc–antigorite boundary, after the destruction of forsterite. Such bulk compositions for peridotite are quantitatively of minor extent in the large ultramafic complexes of orogenic zones (Coleman, 1971), and therefore talc, as compared to brucite, is generally of minor importance as a product of serpentinization. On the other hand, a high-forsterite assemblage would send the path along the forsterite–antigorite boundary, after the destruction of talc, to the forsterite–antigorite–brucite intercept. At this point forsterite is finally destroyed, and the cooling proceeds along the brucite–antigorite boundary to low temperatures.

Controls in serpentinization.—An interesting question immediately raised by the relationships of figure 1 is the control on chrysotile versus

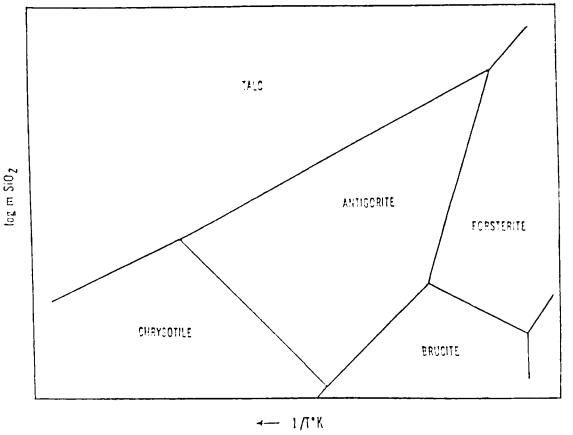

Fig. 8. Schematic diagram of possible stability relations for antigorite and chrysotile.

antigorite development in serpentinization. Because antigorite is characterized by slightly higher SiO_2 content, one might expect it to be a minor and theoretically excluded phase in brucite-bearing serpentinites due to incompatibility with brucite. The forsterite–serpentine boundary of figure 1 would then extend from the talc–antigorite–forsterite point to the brucite–chrysotile–forsterite point. Fields of chrysotile and antigorite might then be separated by a distinct phase boundary, or, perhaps, a field of continuous solid solution might exist. On the other hand, the association brucite–antigorite is observed in many low-grade metamorphic assemblages involving serpentinite, as shown by Trommsdorf and Evans (1974) and others, which suggests that a chrysotile–antigorite stability boundary, if it exists, occurs at a lower temperature than the chrysotile–brucite–forsterite isobaric invariant point. The topology is shown in figure 8. The relations indicate that talc–chrysotile, if stable at all, would be stable only at rather low temperatures and perhaps only in the relatively pure MgO–SiO_2–H_2O system. On the basis of the free energy of hypothetical, pure Mg antigorite ($Mg_{2.825}Si_2O_5(OH)_{3.65}$) given in table 3, the antigorite–brucite–forsterite 1 kb invariant point is at approx 367°C, and the brucite–antigorite–chrysotile and talc–antigorite–chrysotile 1 kb invariant points are at approx 325° and 180°C, respectively.[3] Thus, chrysotile and antigorite have a wide range of stable coexistence. The three reactions are: At + 1.175 B = 2 F + 3 H_2O, C = At + 0.175 B, and 0.117 T + 1.766 C = 2 At. The reader should bear in mind that the antigorite–brucite decomposition curve is not as well established as the corresponding curve for chrysotile. The last two reactions are H_2O-independent, and their steep curves constitute additional boundaries in figure 5. They are not plotted because of space limitations. Although the temperature values calculated for these equilibria are reasonable from the

[3] Evans and others (1976) have also considered these low-temperature relationships in a manuscript that came to our attention when the present paper was in press.

standpoint of metamorphic field relations, the position and slope of the chrysotile–antigorite boundary of figure 8, as well as the positions and slopes of the two curves just mentioned, are very sensitive to small changes in the thermodynamic data used, and the stability of antigorite might extend to appreciably lower temperatures. The temperature calculated for the talc–chrysotile–antigorite intercept, for example, falls well above the range of uncertainty suggested by the downward extrapolation of the talc–antigorite boundary given in figure 1. Salient points of the present discussion are that a stability boundary between antigorite and chrysotile is suggested at low, but geologically reasonable, temperatures and that increasing temperature, increasing aqueous silica activity, and probably higher Fe and Al content, favor the stability of antigorite relative to chrysotile.

In addition to the reactions already discussed, the significance of mineral dissolution reactions in the formation of serpentine should also be appreciated. For forsterite, for example,

$$\text{forsterite} + 4\ H_2O = 2\ Mg^{+2} + H_4SiO_4 + 4\ OH^-$$

or, the equivalent

$$\text{forsterite} + 4\ H^+ = 2\ Mg^{+2} + H_4SiO_4 \qquad (23)$$

Similar reactions can be written for enstatite or other phases present. The individual kinetic character of these reactions and their relative quantitative importance as given by the proportions of olivine and pyroxene in the rock will determine the net loss of Si or Mg in any given case of serpentinization.

To visualize these processes better, the reader may refer to the equilibrium relationships of figure 9. The idealized or stoichiometric dissolution vectors of enstatite and forsterite, although undoubtedly deviating from the real path, are shown and are close to those of talc and chrysotile discussed in the preceding paper (Hemley and others, 1977). The saturation boundaries for enstatite and forsterite, however, are at higher $[Mg^{+2}]/[H^+]^2$ values than for talc and chrysotile, reflecting the fact that enstatite and forsterite are metastable with respect to the latter minerals at this temperature and 1 kb. After intercepting the chrysotile boundary and assuming only minor advancement beyond before crystallization of chrysotile occurs, the forsterite dissolution path moves downward, consuming aqueous silica and producing chrysotile, until the brucite–chrysotile isobaric invariant point is reached. At this point forsterite converts to brucite plus chrysotile at constant solution composition (reaction 24). If there is a net addition of H^+, as with a continuing movement of water through the system, brucite is selectively removed, but at that same $Mg^{+2}/[H^+]^2$ ratio, so long as brucite is present.

The enstatite path follows the opposite course. Enstatite releases silica to produce chrysotile and converts to talc plus chrysotile when the talc–chrysotile point is attained. For the enstatite–forsterite pair, a path intermediate between the two discussed would, of course, result. Talc and

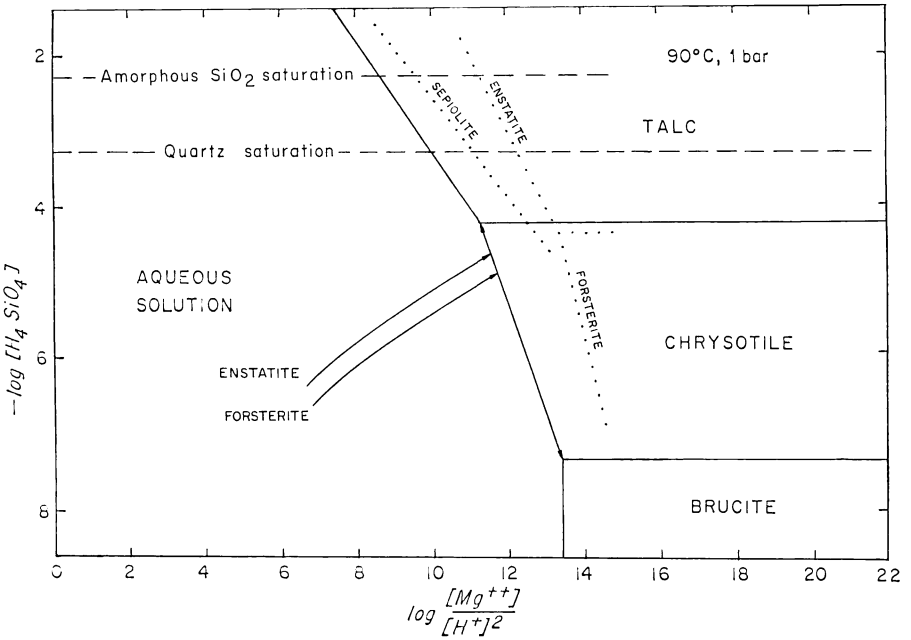

Fig. 9. Stability relations in the MgO–SiO_2–H_2O system as a function of aqueous composition. The vectors show the stoichiometric dissolution paths for forsterite and enstatite. The dotted lines indicate metastable mineral-aqueous solution saturation boundaries for forsterite, enstatite, and sepiolite.

brucite being incompatible, the final assemblage is either brucite–chrysotile, chrysotile, or talc–chrysotile, depending upon the bulk composition of the rock and the Mg and Si lost.

The dissolution reactions have particular significance in an open system because they represent net removal of material and therefore tend to cancel positive volume changes resulting from hydration alone. The concentrations of Mg and Si involved are of the order of the aqueous silica concentrations indicated for the chrysotile field in figure 1, and therefore relatively large volumes of water are implied for sufficient removal of material to maintain the constant bulk volume suggested by some textural studies, for example, in chromites (Thayer, 1966). Rate of removal of material may thus become the rate-controlling step in serpentinization in such places. As pointed out by Hostetler and others (1966), addition of material, namely Si, probably rarely occurs in the large-scale, massive type of serpentinization here being discussed. An important point, however, is that the increase in pressure that would result from hydration, for example, in the end member reaction

$$2 \text{ forsterite} + 3\ H_2O = \text{serpentine} + \text{brucite},\ \Delta V_s \cong 50 \text{ percent}^4 \quad (24)$$

[4] More realistic rock compositions discussed by Hostetler and others (1966) involve volume increases in the region of 40 percent.

would tend to reduce porosity and suppress hydration; also, this increase in pressure would increase mineral solubility slightly in the dissolution process. Reactions of type (23), as well as hydrolytic alteration processes involving primarily the removal of Mg, may therefore be of considerable importance. The problem of volume change in serpentinization has been discussed in some detail by Hostetler and others (1966) for alpine serpentinites, but the evidences for approximate constant volume, in places and on scales where the evidence is more compelling, were not stressed. In short, it seems reasonable to suggest that a volume increase, with its important tectonic implications, is likely as a general rule in the serpentinization process, but in many instances that increase may be relatively small. A similar view has been expressed by Coleman (1971). Constant bulk-volume reactions in cases where ΔV_s is negative obviously have no such constraint. This type of relationship has been discussed previously (Meyer and Hemley, 1967, p. 208).

Although the $[Mg^{+2}]/[H^+]^2$ value of waters associated with serpentinization are defined approximately by the region of stability of brucite, as discussed above, calcium released from pyroxene does not readily become fixed at low temperatures in a solid phase, and the solution should become relatively enriched in calcium hydroxide. In a CO_2-free system, very high pH values could develop. Such waters have apparently been identified and have been discussed by Barnes and O'Neil (1969).

Metamorphic reaction series.—The isochemical cooling and reaction path described above define reaction progress in cases where equilibrium is maintained on cooling in the presence of excess water, that is, at a finite and effective P_{H_2O}. Commonly this is not the case, as water is soon depleted, and most serpentinization, for example, is largely the result of later, low-temperature dissolution and hydration processes operating below the talc–serpentine–forsterite and serpentine–brucite–forsterite dehydration curves. Nevertheless, as in igneous processes, the equilibrium path should be understood as a background for petrologic interpretation. It should be noted that the cooling and reaction sequence described above is similar to that observed in the classical Bowen reaction series for igneous melts. Indeed, the isobaric invariant points discussed could well be called reaction points, exactly analogous to the isobaric peritectic points in silicate melt diagrams.

The reaction sequence and principles described are of fundamental importance to processes of rock-water interaction in general, and particularly to deuteric alteration and retrograde metamorphism. At high temperatures, even in mafic systems, aqueous silica concentrations are seen to be quite high, and this gives rise to hydration and silica-fixation reactions on cooling as the dominant chemical process involving the aqueous phase. Conversely, an Mg-rich residual assemblage, for example, forsterite from enstatite, would also tend to be generated. In quartz-bearing, aluminosilicate rocks the parallel process is, of course, the continuous precipitation of quartz from the migrating aqueous phase. A

significant component of meteoric water may be present in many examples of so-called deuteric alteration, but the reactions discussed would apply regardless of the ultimate source of water. The consequences of cooling, or of differential movement of fluid, at a rate too rapid for maintenance of equilibrium would be the same as in the Bowen reaction series, namely, zoning or armoring of crystals and veins and the development of a fluid phase higher in SiO_2 than the equilibrium value. The increased capability of such a fluid for the formation of the higher silica phases, as in talc veining and alteration of mafic rocks, is obvious.

SUMMARY AND CONCLUSIONS

High-temperature phase equilibria in the system MgO–SiO_2–H_2O have been investigated through consideration of the silica-dependent reactions of the system. Supplementing the thermodynamic relations given in the previous paper (Hemley and others, 1977), Gibbs free energies of formation for antigorite, anthophyllite, and enstatite have been obtained. The pressure-temperature net for the more significant phases in the system is presented.

A major aim of the paper has been to illustrate the manner in which experimentation and theory can contribute to a better understanding of petrologic processes that involve changes in bulk composition, while at the same time considering the related isochemical transformations. The log concentration versus 1/T plots presented illustrate such applications, whether the processes be of metamorphic, late-magmatic, or hydrothermal origin. Contact metamorphism/metasomatism, rock alteration, the process of serpentinization, controls on serpentinite mineralogy, and the stability relations between chrysotile and antigorite are discussed.

The chemical constraints associated with the various equilibria studied, particularly when the effects of changing pressure are considered, help to clarify PT relationships for the associated thermal dehydration reactions and to remove some of the ambiguity inherent in a conventional pressure-temperature (Schreinemachers) analysis. For isothermal-isobaric processes, activity-activity diagrams are, of course, useful, but care should be taken to consider reactions appropriate to the real process involved lest serious errors develop in the analysis. This general requirement for components of the aqueous phase should be kept in mind in the use of chemical potential diagrams and in the evaluation of such diagrams in the literature as applied to the interpretation of geologic processes.

In isochemical heating or cooling, evolution of the system occurs via the silica-dependent reactions and a change in mineral assemblage at successive isobaric invariant points. A mineral reaction series analogous to that of igneous melt systems at peritectic points is thus illustrated. The relationships depicted are of particular significance to deuteric alteration, retrograde metamorphism, and hydrothermal vein formation.

ACKNOWLEDGMENTS

The authors are grateful to P. B. Barton, Jr., C. L. Christ, and E-an Zen of the U.S. Geological Survey and J. V. Chernosky of the University of Maine for their critical reviews of this paper. The comments of J. R. Fisher and J. L. Haas of the Survey and of B. W. Evans of the University of Washington on various aspects of the paper are also appreciated. We wish to thank Leonard Shapiro and S. D. Botts, also of the U.S. Geological Survey, for mineral analyses and for many of the aqueous silica analyses.

REFERENCES

Barnes, Ivan, and O'Neil, J. R., 1969, The relationships between fluids in some fresh alpine-type ultramafic and possible modern serpentinization, western United States: Geol. Soc. America Bull., v. 80, p. 1947-1960.

Brown, George, 1961, The X-ray identification and crystal structures of clay minerals: Mineralog. Soc. London, 544 p.

Chernosky, J. V., Jr., 1974, The stability field of anthophyllite—an experimental redetermination: Geol. Soc. America Abs. with Programs, v. 6, no. 7, p. 687.

Christ, C. L., Hostetler, P. B., and Siebert, R. M., 1973, The activity product constant of sepiolite: Am. Jour. Sci., v. 278, p. 65-83.

Coleman, R. G., 1971, Petrologic and geophysical nature of serpentinite: Geol. Soc. America Bull., v. 82, p. 897-918.

Crerar, D. A., and Anderson, G. M., 1971, Solubility and solution reactions of quartz in dilute hydrothermal solutions: Chem. Geology, v. 8, p. 107-122.

Deer, W. A., Howie, R. A., and Zussman, J., 1962, Rock forming minerals, v. 2: New York, John Wiley & Sons, 270 p.

Evans, B. W., Johannes, Wilhelm, Oterdoom, H., and Trommsdorf, Volkmar, 1976, Stability of chrysotile and antigorite in the serpentinite multisystem: Schweizer. min. pet. Mitt., v. 56, p. 79-93.

Evans, B. W., and Trommsdorf, Volkmar, 1974, Stability of enstatite + talc, and CO_2-metasomatism of metaperidotite, Val d'Efra, Lepontine Alps: Am. Jour. Sci., v. 274, p. 274-296.

Faust, G. T., and Fahey, J. J., 1962, Studies of the natural phases in the system MgO–SiO_2–H_2O and the systems containing the cogeners of magnesium: U.S. Geol. Survey Prof. Paper 384-A, 92 p.

Fisher, J. R., and Zen, E-an, 1971, Thermochemical calculations from hydrothermal phase equilibrium data and the free energy of H_2O: Am. Jour. Sci., v. 270, p. 297-314.

Frost, B. R., 1975, Contact metamorphism of serpentinite, chloritic blackwall and rodingite at Paddy-Go-Easy Pass, Central Cascades, Washington: Jour. Petrology, v. 16, pt. 2, p. 272-313.

Greenwood, H. J., 1963, The synthesis and stability of anthophyllite: Jour. Petrology, v. 4, p. 317-351.

———— 1971, Anthophyllite, corrections and comments on its stability: Am. Jour. Sci., v. 220, p. 151-154.

Gustafson, L. B., and Hunt, J. P., 1975, The porphyry copper deposit at El Salvador, Chile: Econ. Geology, v. 70, p. 857-912.

Hemley, J. J., Montoya, J. W., Christ, C. L., and Hostetler, P. B., 1977, Mineral equilibria in the MgO–SiO_2–H_2O system: I. Talc–chrysotile–forsterite–brucite stability relations: Am. Jour. Sci., v. 277, p. 322-351.

Hemley, J. J., Shapiro, L., Shaw, D. R., and Luce, R. W., 1975, Stability relations of anthophyllite: Geol. Soc. America Abs. with Programs, v. 7, no. 7, p. 1109.

Hostetler, P. B., Coleman, R. G., Mumpton, F. A., and Evans, B. W., 1966, Brucite in alpine serpentinites: Am. Mineralogist, v. 51, p. 75-98.

Johannes, Wilhelm, 1975, Zur Synthese und thermischen Stabilität von Antigorit: Fortschr. Mineralogie, v. 53, p. 36.

Kelley, K. K., 1960, Contributions to data on theoretical metallurgy, XIII: High-temperature heat content, heat capacity, and entropy data for the elements and inorganic compounds: U.S. Bur. Mines Bull. 584, 232 p.

King, E. G., Barany, R., Weller, W. W., and Pankratz, L. B., 1967, Thermodynamic properties of forsterite and serpentine: U.S. Bur. Mines, Rept. Inv. 6962, 19 p.

Korzhinsky, D. S., 1962, Mineral paragenesis of the MgO–SiO_2–H_2O–CO_2 and the water-carbon dioxide regimen in metamorphism: Internat. Geol. Rev., v. 4, p. 789-816.

Kunze, Gunther, 1956, Die gewellte Struktur des Antigorits, I: Zeitschr. Kristallographie, v. 108, p. 82-107.

———— 1961, Antigorit, strukturtheoretische Grundlagen und ihre praktische Bedeutung für die weitere Serpentin-Forschungs: Fortschr. Mineralogie, v. 39, p. 206-324.

Larsen, E. S., 1928, A hydrothermal origin of corundum and albitite bodies: Econ. Geology, v. 23, p. 398-433.

Latimer, W. M., 1952, The oxidation states of the elements and their potentials in aqueous solutions: Englewood Cliffs, N.J., Prentice-Hall Inc., 392 p.

Mel'nik, Yu. P., and Onopriyenko, V. L., 1969, Termodinamicheskiye svoystva antofillita, *in* Konstitutsiya i Svoysta Mineralova, 3, Kiyev: Akad. Nauk. Ukrain. SSR, v.46-45 (English translation — Thermodynamic properties of anthophyllite: Geochem. Internat., 1969, v. 6, p. 994-999).

Meyer, Charles, and Hemley, J. J., 1967, Wall rock alteration, *in* Barnes, H., ed., Geochemistry of hydrothermal ore deposits: New York, Holt, Rinehart and Winston, 670 p.

Page, N. J., 1968, Chemical differences among the serpentine "polymorphs": Am. Mineralogist, v. 53, p. 201-215.

Page, N. J., and Coleman, R. G., 1967, Serpentine-mineral analyses and physical properties: U.S. Geol. Survey Prof. Paper 575-B, p. B103-B107.

Robie, R. A., and Waldbaum, D. R., 1968, Thermodynamic properties of minerals and related substances at 298.15°K and one atmosphere and at higher temperatures: U.S. Geol. Survey Bull. 1259, 256 p.

Singer, A., and Norrish, K., 1974, Pedogenic palygorskite occurrences in Australia: Am. Mineralogist, v. 59, p. 508-517.

Thayer, T. P., 1966, Serpentinization considered as a constant-volume metasomatic process: Am. Mineralogist, v. 51, p. 685-710.

Trommsdorff, Volkmar, and Evans, B. W., 1972, Progressive metamorphism of antigorite schist in the Bergell Tonalite aureole (Italy): Am. Jour. Sci., v. 272, p. 423-437.

———— 1974, Alpine metamorphism of peridotitic rocks: Schweizer. min. pet. Mitt., v. 54, p. 333-352.

Whittaker, E. J. W., and Wicks, F. S., 1970, Chemical difference among serpentine "polymorphs": a discussion: Am. Mineralogist, v. 55, p. 1025-1047.

Wollast, R., Mackenzie, F. T., and Bricker, O. P., 1968, Experimental precipitation and genesis of sepiolite at earth-surface conditions: Am. Mineralogist, v. 53, p. 1645-1662.

Zen, E-an, 1971, Comments on the thermodynamic constants and hydrothermal stability relations of anthophyllite: Am. Jour. Sci., v. 270, p. 136-150.

Zen, E-an, and Chernosky, J. V., Jr., 1976, Correlated free energy values of anthophyllite, brucite, clinochrysotile, enstatite, forsterite, quartz and talc: Am. Mineralogist, v. 61, p. 1156-1166.